# Simulation and Optimization of a Solar Based Trigeneration System Incorporating PEM Electrolyzer and Fuel Cell

## Ehsanolah Assareh[a], Farshid Mohammadi Bouri[a], Behzad Azizimehr[b], Rahim Moltames[c, *]

[a]Department of Mechanical Engineering, Dezful Branch, Islamic Azad University, Dezful, Iran
[b]Department of Mechanical Engineering, West Tehran Branch, Islamic Azad University, Tehran, Iran
[c]Department of Energy Engineering, Energy Systems Engineering, Sharif University of Technology

## Abstract

In addition to simultaneously supplying heat and electricity, CCHP systems also provide the cooling demand of the buildings. The input energy of this system can be supplied from renewable energy sources such as solar energy, geothermal energy and so on. Compared to conventional power generation systems, cogeneration systems have higher energy efficiency, lower pollutant production, and higher reliability. In this paper, a solar-powered CCHP system equipped with a PEM electrolyzer and fuel cell is simulated and optimized. The combination of the PEM electrolyzer and the fuel cell is used in order to provide sustainable heat and electricity. For this purpose, the electrical power produced in the cycle is converted to hydrogen by the electrolyzer as the demand for electricity is low and converted to electricity by the fuel cell when needed. The results of system optimization showed that energy efficiency and exergy efficiency increased by 22.32% and 8.61% in the first scenario, respectively. Moreover, the total cost rate of the system is reduced by 6.65% in the second scenario.

**Keywords:** Solar energy, cogeneration, CCHP, electrolyzer, fuel cell, optimization

## 1. Introduction

CCHP system is a developed concept of CHP systems that is applied in large scale power generating units. CCHP systems have been developed in order to resolve the problem of low efficiency in conventional systems that provide heat, cooling, and electric power separately. CCHP systems provide a large amount of electrical and thermal energy demand of the buildings simultaneously using thermal recovery. The input energy of these systems can be supplied from renewable energy sources such as solar energy, geothermal energy and so on. Compared to conventional power generation systems, electricity, heat, and electricity co-generation systems have higher energy efficiency, lower pollutant production, and higher reliability. Higher efficiency of these systems means less initial energy consumption to produce a sustainable amount of output energy. Researchers have done a lot of research on simulating and optimizing CCHP cogeneration systems. In this

regard, Wang and his colleagues [1] proposed a small-scale fuel cell-based cogeneration system to meet the cooling, heating and power requirements of home applications. Their system consists of a dual-effect lithium bromide fuel cell, boiler and absorber chiller that uses the dissipated heat of the fuel cell to cool and heat. Using parametric analysis of the system, they showed that the equivalence ratio and fuel consumption factor had the greatest impact on the efficiency of the system and the ratio of thermal to electrical power. In 2004, Tamir and his colleagues [2] thermoeconomically evaluated a cogeneration system. The system was based on a reciprocating engine that runs on natural gas and was capable of producing 1900 kW. In order to analyze the system from a thermochemical point of view, they first calculated the exergy values of each flow and the destroyed exergy of each system, then evaluated their investment and operating costs, and made suggestions to improve the

performance of the components. Cardona and his colleagues [3] optimized CCHP power plants for public buildings using the thermoeconomic approach. They showed that the CCHP system is a safe and competitive system and can be a suitable option for use in hospitals. Deng and his colleagues [4] thermoeconomically analyzed a cogeneration system. The results of the parametric analysis showed that lower inlet temperature of the absorption chiller results in lower product cost rate and is effective in the overall system efficiency. Ghaebi and his colleagues [5] optimized a cogeneration system using the genetic

algorithm and TRR methods. They determined the optimum value of the design parameters using the genetic metaheuristic algorithm, and it was observed that the optimal objective function improves up to 15% compared to the base case. In this paper, a solar-based CCP system is simulated and optimized. The feasibility of using the PEM electrolyzer and fuel cell for sustainable energy production is investigated for the first time in this paper. PSO algorithm is used to optimize the system and MATLAB software is used in order to simulate and optimize the system.

## 2. Methodology

Fig. 1 shows the detailed layout of the system presented in this paper. As shown in Fig. 1, the input energy of the system is provided using the solar concentrator system. The power generation system produces electric power using the generator. A part of this power enters the electrolyzer in order to produce

hydrogen. Using the ejector leads to supply the cooling demands. If needed, the produced hydrogen is used to produce electricity and heat incorporating the PEM fuel cell. the detail concepts of each part will be discussed later.
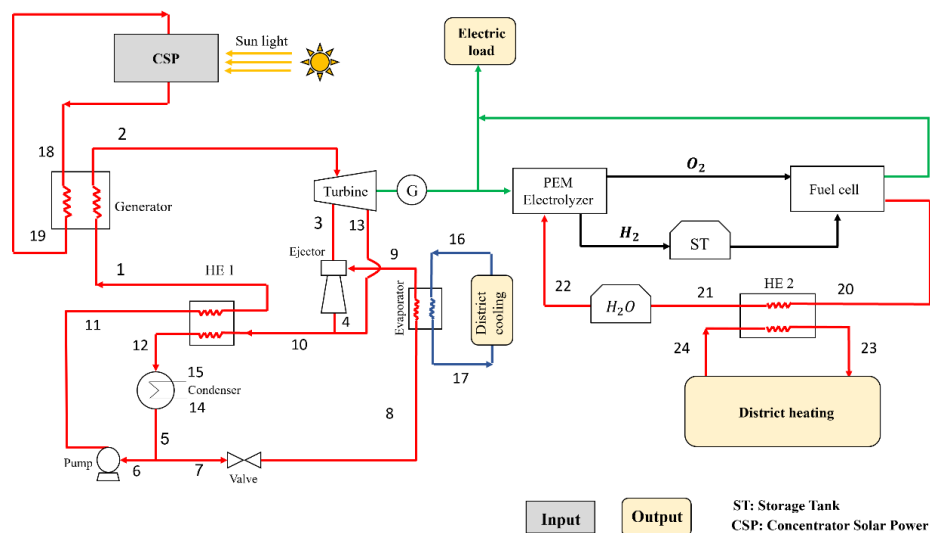


**Figure 1. Scheme of the CCHP proposed in this paper**

## 3. Fuel cell model

The Proton-exchange membrane fuel cell is an electrochemical cell fed by hydrogen gas. Hydrogen enters the anode side of the fuel cell and is oxidized and the inlet oxygen is reduced to the fuel cell cathode. During the hydrogen oxidation process, the released proton travels to the cathode through the proton

exchange membrane, while the electron released through the hydrogen oxide is unable to pass through the membrane. Therefore, the electron generates an electrical current moving across the outer circuit. The fuel cell equations are written as follows [6]:

**Anode:**
$$H_2 \rightarrow 2H^+ + 2e^-$$

**Cathode:**
$$2H^+ + \frac{1}{2}O_2 + 2e^- \rightarrow H_2O$$

**Total reaction:**
$$\frac{1}{2}O_2 + H_2 \rightarrow H_2O + heat$$

The electromotive force or open-circuit voltage in a fuel cell is calculated as follows [7]:

$$E = -\frac{\Delta G_f}{2F} \qquad (1)$$
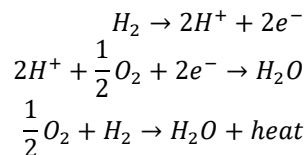
where $E$ is the open-circuit voltage of the cell in volts, $\Delta G_f$ is Gibbs free energy in joule/mol, and $F$ is the Faraday constant (equal to 96.485 ° C/mol). The actual voltage of the fuel cell is equal to the sum of the Nernst voltage, activation voltage, ohmic losses voltage, and concentration voltage [8]:

$$V_{FC} = E_N - (V_a + V_o + V_c) \qquad (2)$$

The Nernst voltage is calculated using the temperature and pressure of the fuel cell as follows [9]:

$$E_N = E° - 0.85 \times 10^{-3}(T_{cell} - 298.15) + 4.31 \times 10^{-5} T_{cell}\left[\ln\left(P_{H_2}^{contact}\right) + 0.5 \times \ln\left(P_{O_2}^{contact}\right)\right] \qquad (3)$$

where $E^0$ is the electromotive force at standard temperature and pressure (=1.229 V). The activation voltage causes the actual voltage drop and can be significant at low temperatures and pressures, which can be calculated by the following equation [10]:

$$V_a = \delta_1 + \delta_2 T_{cell} + \delta_3 \times \ln\left(1.97 \times 10^{-7} P_{O_2} \times \exp\left(\frac{498}{T_{cell}}\right)\right) + \delta_4 T_{cell} \times \ln(I) \qquad (4)$$

where:
$\delta_1 = -0.948$
$\delta_2 = -0.00286 + 0.0002 \times \ln(A_{cell}) + 4.3 \times 10^{-5} \times \ln(9.174) \times 10^{-7} P_{H_2} \exp\left(\frac{-77}{T_{cell}}\right)$
$\delta_3 = 7.6 \times 10^{-5}$
$\delta_4 = -1.93 \times 10^{-4}$

Ohmic losses are due to the electrical resistance created by the electrolyte. According to Ohm's law, the voltage of ohmic losses is calculated according to the following equation:

$$V_o = IR \qquad (5)$$

The internal resistance of the fuel cell is obtained from the following equation:

$$R = \frac{r_m l_m}{A_{cell}} \qquad (6)$$

where $l_m$ is the thickness of the membrane and $r_m$ is obtained from the following equation [11]:

$$r_m = \frac{181.6\left[1 + 0.03\left(\frac{I}{A_{call}}\right) + 0.062\left(\frac{I}{303}\right)^2\left(\frac{}{A_c}\right.\right.}{\left[11.866 - 3\left(\frac{I}{A_{call}}\right)\exp\left(4.18\left(\frac{T_{cell} - 30}{T_{cell}}\right)\right.\right.} \qquad (7)$$
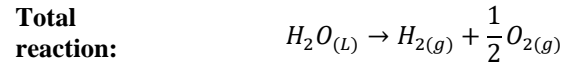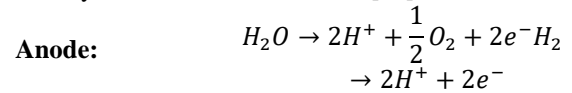
The concentration voltage is caused by changes in the concentration of the reactants at the electrode surface and is calculated by the following equation:

$$V_c = m \times \exp(ni) \qquad (8)$$

where $m = 3 \times 10^{-5}$ and $n = 8$ and $i$ is the current density.

***PEM electrolyzer model***
The reactions at the cathode and anode of a PEM electrolyzer are written as follows [12]:

**Anode:** $\quad H_2O \rightarrow 2H^+ + \frac{1}{2}O_2 + 2e^- H_2 \rightarrow 2H^+ + 2e^-$

**Cathode:** $\quad 2H^+ + 2e^- \rightarrow H_2$

**Total reaction:** $\quad H_2O_{(L)} \rightarrow H_{2(g)} + \frac{1}{2}O_{2(g)}$

Based on the Gibbs free energy of reaction, there is a reversible voltage for the PEM electrolyzer. This voltage corresponds to the ideal electrolyzer cell in isothermal reversible conditions. Gibbs free energy is defined as [13]:

$$\Delta G = \Delta H - T\Delta S \qquad (9)$$

Where $\Delta H$ is the enthalpy change in J/mole, $\Delta S$ is the enthalpy changes in J/mole, and $T$ is the temperature in Kelvin. Under ideal conditions, the heat generated during the reaction is continuously excreted from the system, so the system temperature does not change. The amount of energy released is equal to the change in entropy and temperature. The reversible potential is obtained by the following equation:

$$V_0 = -\frac{\Delta G}{2F} \qquad (10)$$

The open-circuit voltage for the PEM electrolyzer is obtained using the Nernst equation:

$$V_0 = 1.229 - 8.5 \times 10^{-3}(T_{PEM} - 298) \qquad (11)$$

The voltage for a single PEM electrolyzer cell is defined as follows:

$$V = V_0 + V_{act.a} + V_{act.c} + V_{ohm} \qquad (12)$$

Where $V_{act,a}$ is the activation voltage drop at the anode, $V_{act,c}$ is the activation voltage drop at the cathode and $V_{ohm}$ is the ohmic loss voltage in volts.

The activation energy on both sides of the cathode and the anode is calculated as follows:

$$V_{act.i} = \frac{RT}{F} sinh^{-1}\left(\frac{J}{2J_{0.i}}\right) \tag{13}$$

Where $J_{0,i}$ is the anode/cathode current density in A/cm2 and is obtained by:

$$J_{0.i} = J_i^{ref} exp\left(-\frac{V_{act.i}}{RT}\right) \tag{14}$$

The ohmic voltage drop due to the membrane resistance is the electrolyzer resistance to proton transfer and is a function of the membrane thickness (*L*) in meters, the ion conductivity of the ion exchange membrane ($\sigma_{mem}$) in $1/(\Omega.cm)$, and current density (*J*) in A/cm2 which can be calculated by the following equations [14], [15], [16]:

$$V_{ohm} = J R_{PEM} \tag{15}$$

$$R_{PEM} = \int_0^D \frac{dx}{\sigma_{mem}[\lambda(x)]} \tag{16}$$

$$\lambda(x) = \frac{\lambda_a - \lambda_c}{D}x + \lambda_c \tag{17}$$

$$\sigma_{mem}[\lambda(x)] = [0.5139\lambda(x) \tag{18}$$
$$- 0.326]exp\left[1268\left(\frac{1}{303} - \frac{1}{T}\right)\right]$$

The mass flow rate of hydrogen produced in the electrolyzer is obtained from the following equation [17]:

$$\dot{N}_{H_2.out} = \frac{J}{2F} = 2\dot{N}_{H_2O.reacted} \tag{19}$$

### Energy Analysis

The conservation of energy and mass laws are used in order to energy analysis of the system. Each component in the system is considered as a control volume. For a control volume with input *i* and output *o*, mass and energy conservation laws can be written as follows [18]:

$$\sum \dot{m}_i = \sum \dot{m}_o \tag{20}$$

$$\sum \dot{Q} = \sum \dot{W} = \sum \dot{m}_o h_o - \sum \dot{m}_i h_i \tag{21}$$

The following assumptions are considered in energy analysis:
- ✓ The system is in steady-state and the pressure drop in pipes, evaporators, and heat exchangers is ignored.
- ✓ The flow inside the valve is considered to be isentropic.
- ✓ The condenser outlet state is saturated liquid; on the other hand, the evaporator outlet state is assumed to be saturated vapor.

- ✓ Potential and kinetic energies are ignored.

### Exergy Analysis

Exergy is the maximum work you can obtain from the energy. In the exergy analysis of the present study, the following assumptions are taken into account:
- ✓ Only physical exergies are considered for flows.
- ✓ Due to the low velocities, the potential and kinetic energies are neglected.

Applying the first and second laws of thermodynamics, exergy equations can be calculated as follows [19], [20]:

$$\dot{E}_Q + \sum_i \dot{m}_i e_i = \sum_e \dot{m}_e e_e + \dot{E}_W + \dot{E}_D \tag{22}$$

$$\dot{E}_Q = \left(1 - \frac{T_0}{T}\right)\dot{Q} \tag{23}$$

$$\dot{E}_W = \dot{W} \tag{24}$$

where $\dot{E}_Q$ and $\dot{E}_W$ are heat transfer exergy and work exergy, respectively.

The exergy entering the system originates from the sun. It is assumed that the sun is a black body; therefore, the exergy absorbed by the collectors is calculated by the following equation:

$$\dot{Ex}_S = G_t A_C \left(1 + \frac{1}{3}\left(\frac{T_0}{T_s}\right)^4 - \frac{4}{3}\left(\frac{T_0}{T_s}\right)\right) \tag{25}$$

where $T_{sun}$ is the sun temperature (=6000 K). The thermal efficiency of the system is obtained from the ratio of the energy produced by the system to the input energy of the system in percent (the incoming solar radiation to the receiver):

$$\eta_{Th} = \frac{W_{electrical} + Q_{heat} + Q_{cold}}{Q_r} \times 100 \tag{26}$$

The exergy efficiency is also defined as the ratio of output exergy to the input exergy in percent:

$$\eta_{Ex} = \frac{W_{electrical} + Ex_{heat} + Ex_{cold}}{Ex_S} \times 100 \tag{27}$$

### Economic Analysis

The costs of the system include investment cost ($\dot{Z}_k^{Cl}$) and maintenance cost ($\dot{Z}_k^{OM}$). The sum of these two terms is represented by two terms $\dot{Z}_k$. The cost of maintenance for the entire system life is estimated at one percent of the total investment cost.

$$\dot{Z}_k = \dot{Z}_k^{Cl} + \dot{Z}_k^{OM} \tag{28}$$

The investment costs of each component are shown in Table 1.

**Table 1. investment cost of each component used in the combined system**

| Component | Equation | Eq. number |
|---|---|---|
| Solar concentrator | $\dot{Z}_{CSP} = 550 A_{concentrator}$ | (29) |
| Heat exchangers | $Z_{HE}(\$) = 130 \left( \frac{A_{HE}}{0.093} \right)^{0.78}$ | (30) |
| Turbine | $Log_{10}(Z_T)(\$) = 2.6259 + 1.4398\, log_{10}(\dot{W}_T) - 0.1776 \left[ Log_{10}(\dot{W}_T) \right]^2$ | (31) |
| Pump | $Z_P(\$) = 3540 \dot{W}_P^{0.71}$ | (32) |
| PEM electrolyzer | $Z_{elec}(\$) = 1000 W_{elec}$ | (33) |
| PEM fuel cell | $Z_{FC}(\$) = 1000 W_{FC}$ | (34) |

## 4. Optimization

The optimization of the system in this paper is carried out using Particle Swarm Optimization (PSO) algorithm incorporating MATLAB software. The flowchart of the PSO algorithm used in this paper is shown in Fig. 2. For the proposed system in this paper, the objective function consists of three parameters representing the system performance including energy or thermal efficiency, exergy efficiency, and cost rate. The mathematical model of system optimization is shown in the following equations:

$$Max\ F(T_2, \eta_r, T_6)$$
$$= w_1 \times \eta_{th} + w_2 \times \eta_{ex} \quad (35)$$
$$+ w_3(1 - Z_{total})$$
$$0 \le w_1, w_2, w_3 \le 1 \quad (36)$$

$$w_1 + w_2 + w_3 = 1 \quad (37)$$

Two scenarios are taken into account in order to evaluate the system performance in different optimization criteria. In the first scenario, w1 and w2 are both considered as 0.45 and w3 is considered as 0.1 which means that improving the energy and exergy efficiencies is more important than decreasing the cost rate of the system. On the other hand, in the second scenario, w1 and w2 are both considered as 0.2 and w3 is considered as 0.6 which means that decreasing the cost rate of the system is more important than increasing the energy and exergy efficiencies. The feasible range of decision variables is shown in Table 2.
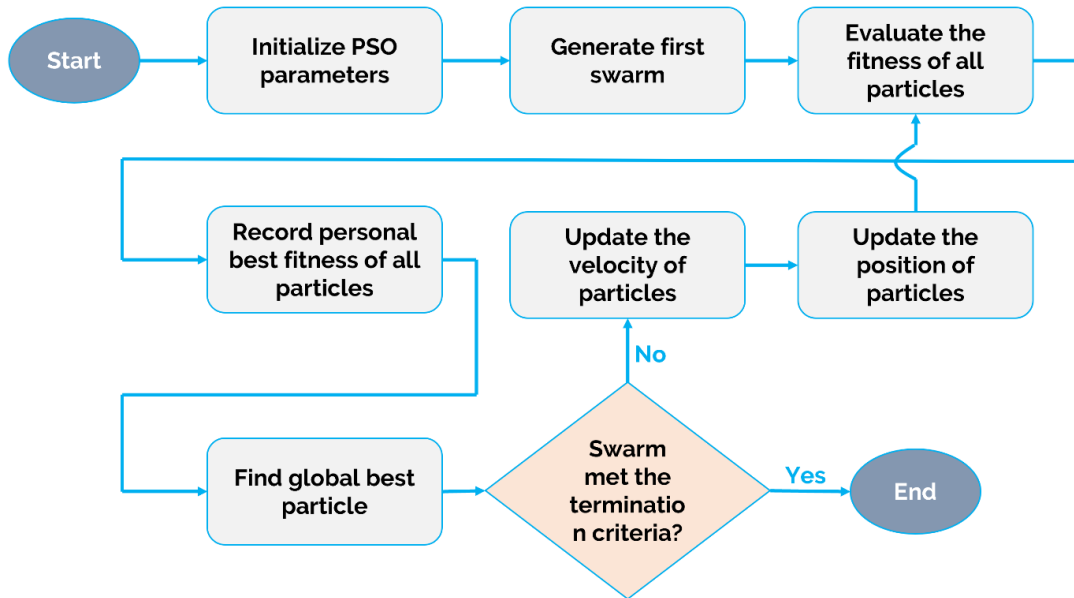


**Figure 2. PSO algorithm flowchart**

**Table 2. The feasible range of decision variables**

| Decision variable | Range |
|---|---|
| Turbine inlet temperature (℃) | $120 \leq T_2(℃) \leq 150$ |
| Receiver efficiency (%) | $60 \leq \eta_r(\%) \leq 85$ |
| Condenser outlet temperature (℃) | $20 \leq T_6(℃) \leq 40$ |

## 5. Results and discussion
### *Validation*

The validation of the present work is done by comparing the results of the system simulation for the ejector cycle with those of the Ref. [21] at different points of the cycle and also, by comparing the electrolyzer performance with the results of the simulation presented in Ref. [13]. Table 2 shows the thermodynamic characteristics of the system cycle compared to the system reviewed in Ref. [21]. The Comparison of the values given in Table 3 indicates the validity of the present work. The slight difference in the values of the parameters is also related to the differences in the software library (thermodynamic properties of the different fluids).

**Table 3. Thermodynamic properties of different points of the ejector cycle (a) compared to those of the Ref. [21] (b)**

| Point | $T$ (℃) | | $P$ $(kPa)$ | | $h$ $(kJ/kg)$ | | $s$ $(kJ/kgK)$ | | $\dot{m}$ $(kg/s)$ | |
|---|---|---|---|---|---|---|---|---|---|---|
| | b | a | b | a | b | a | b | a | b | a |
| 1 | 59.94 | 63.61 | 0.7 | 0.7 | 261.69 | 265.63 | 1.202 | 1.214 | 4.549 | 4.948 |
| 2 | 130 | 130 | 0.7 | 0.7 | 246.95 | 466.96 | 1.762 | 1.761 | 4.549 | 4.948 |
| 3 | 98.98 | 98.98 | 0.22 | 0.22 | 448.59 | 448.60 | 1.773 | 1.772 | 1.765 | 1.779 |
| 4 | 98.98 | 110.7 | 0.0914 | 0.09139 | 443.54 | 459.47 | 1.805 | 1.847 | 1.902 | 2.009 |
| 5 | 25 | 25 | 0.0914 | 0.09139 | 225.14 | 225.15 | 1.088 | 1.087 | 4.549 | 4.708 |
| 6 | 25 | 25 | 0.0914 | 0.09139 | 225.14 | 225.15 | 1.088 | 1.087 | 4.549 | 4.948 |
| 7 | 25 | 25 | 0.0914 | 0.09139 | 225.14 | 225.15 | 1.088 | 1.087 | 0.137 | 0.210 |
| 8 | -5 | -5 | 0.0258 | 0.0258 | 225.14 | 225.15 | 1.094 | 1.094 | 0.137 | 0.210 |
| 9 | -5 | -5 | 0.0258 | 0.0258 | 378.44 | 378.44 | 1.666 | 1.665 | 0.137 | 0.210 |
| 10 | 83.41 | 92.54 | 0.0914 | 0.09139 | 438.67 | 445.55 | 1.792 | 1.810 | 4.549 | 4.708 |
| 11 | 25.35 | 25.34 | 0.7 | 0.7 | 225.69 | 225.70 | 1.088 | 1.088 | 4.549 | 4.948 |
| 12 | 35.35 | 35.34 | 0.0914 | 0.09139 | 403.75 | 403.76 | 1.687 | 1.686 | 4.549 | 4.708 |

Figure 3 shows the current density variation with the voltage of the electrolyzer calculated in this paper. On the other hand, Fig. 4 shows the results obtained from the electrolyzer performance of Ref. [13]. The comparison of these figures indicates the validity of this work.
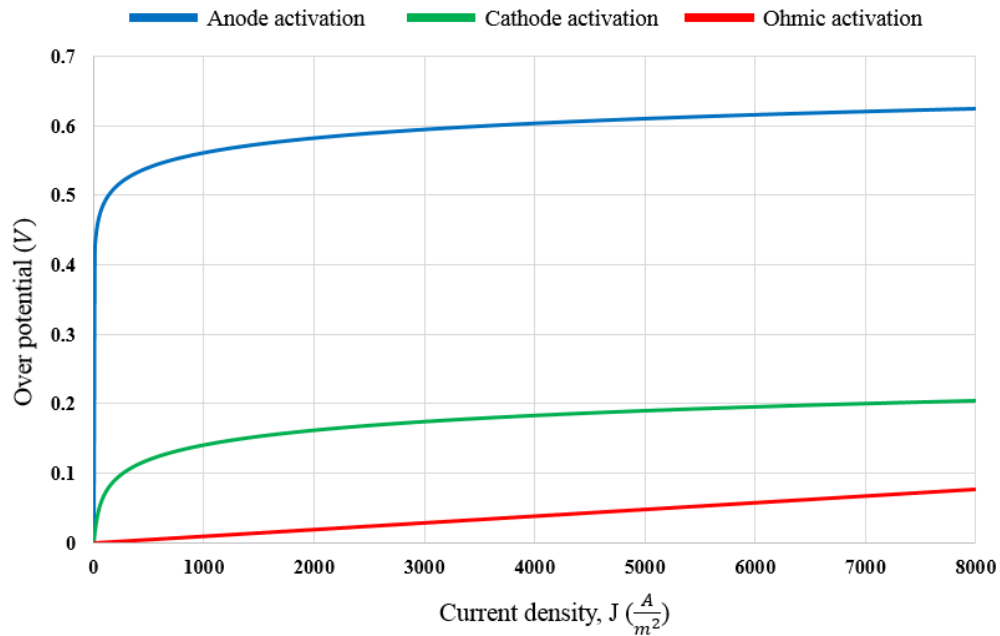
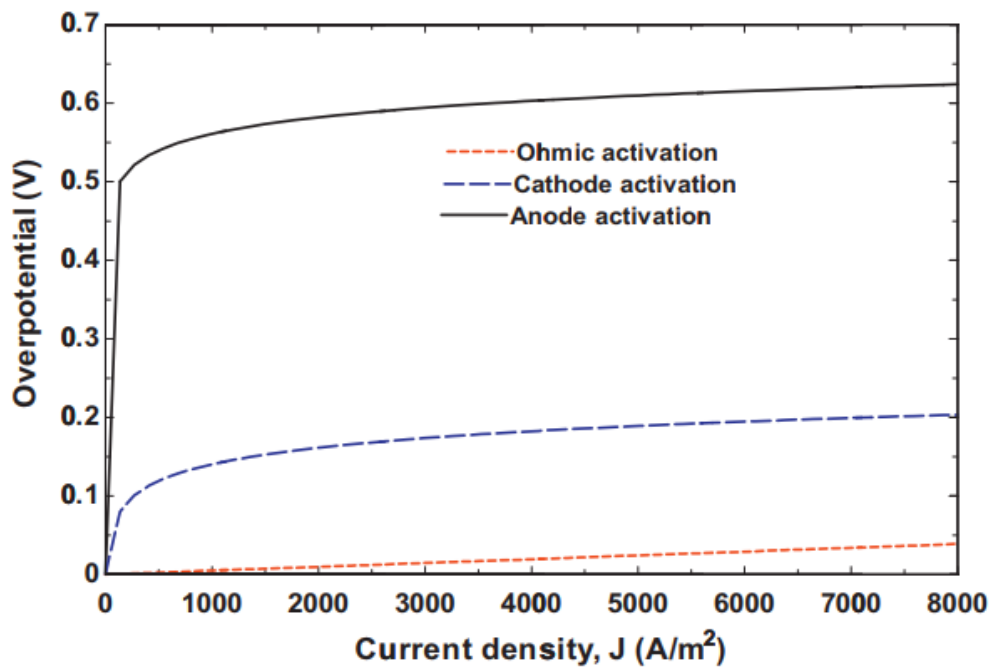**Figure 3. Current density vs voltage calculated in this paper**



**Figure 4. Current density vs voltage calculated in Ref.** [13]

## 7. System performance

Applying power and efficiency equations results in the system performance which is shown in Table 4.

**Table 4. System performance**

| Parameter | Value | Unit |
|---|---|---|
| Turbine power production | 964.14 | kW |
| Pump consumption | 20.22 | kW |
| Total power production | 943.92 | kW |
| Energy efficiency | 9.63 | % |
| Exergy efficiency | 63.48 | % |
| Hydrogen production rate | 2.8 | g/s |
| System total cost rate | 140.41 | $/h |

## 8. Effect of turbine inlet temperature

The effect of the turbine inlet temperature on the objective functions (energy efficiency, exergy efficiency, and cost rate) is shown in Figures 5, 6, and 7, respectively. As shown in Figure 5, increasing the inlet temperature of the turbine increases energy efficiency, which is due to an increment in system output for the constant input energy. The same argument holds for increasing the exergy efficiency of the system (Figure 6). On the other hand, increasing the system output energy also leads to an increase in the capacity of the system components, which in turn results in an increase in the cost of the system (Figure 7).
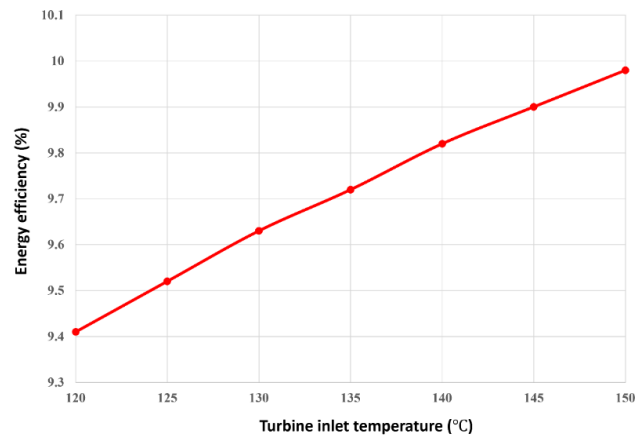


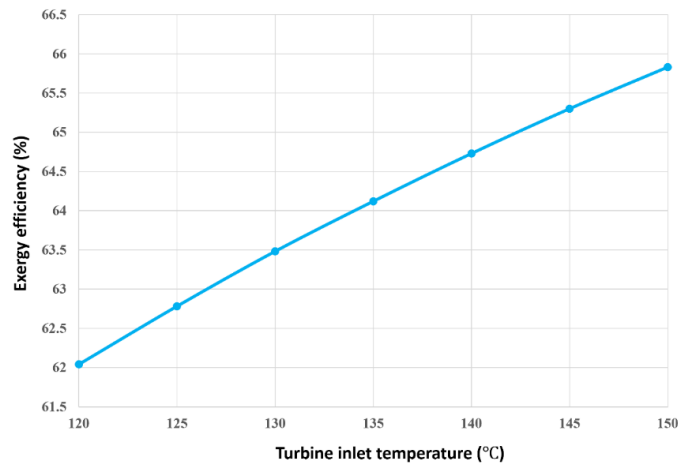**Figure 5. effect of turbine inlet temperature on energy efficiency**



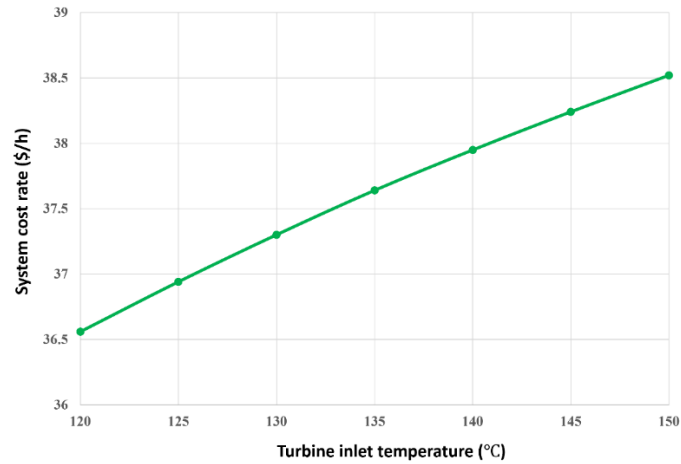**Figure 6. effect of turbine inlet temperature on exergy efficiency**

671

**Figure 7. effect of turbine inlet temperature on the system cost rate**

### 9. Effect of receiver efficiency

The effect of the receiver efficiency on the objective functions (energy efficiency, exergy efficiency, and cost rate) is shown in Figs. 8, 9 and 10, respectively. As shown in Fig. 8, increasing the receiver efficiency increases the energy efficiency due to the decrease in input energy of the system for constant output energy. Increasing the receiver efficiency does not affect the exergy efficiency of the system because increasing the receiver efficiency increases the input and output exergy of the system simultaneously (Fig. 9). On the other hand, increasing the system output energy increases the capacity of the system components, which in turn results in an increase in the cost of the system (Fig. 10).
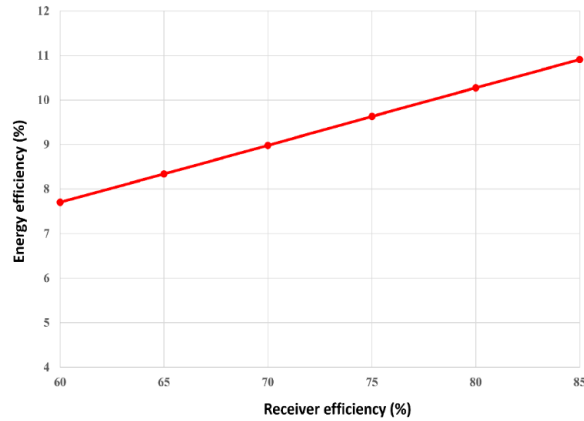


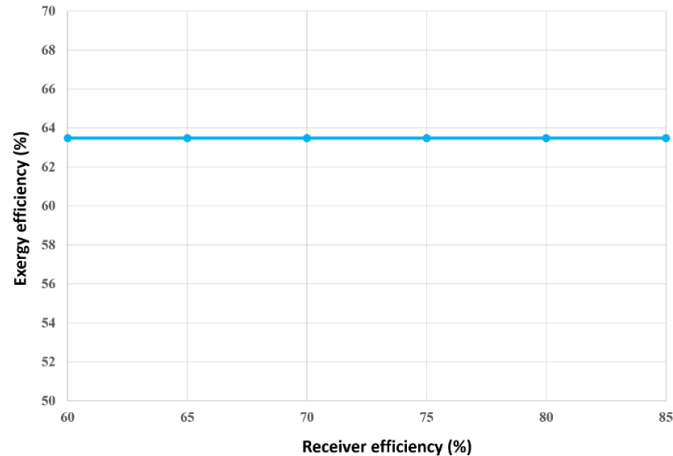**Figure 8. effect of receiver efficiency on energy efficiency**



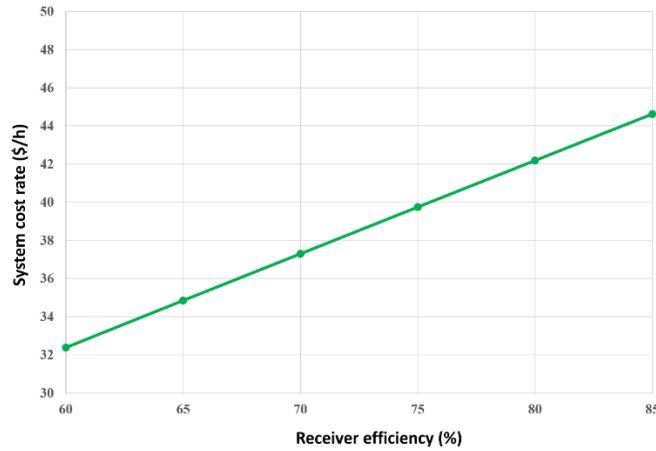**Figure 9. effect of receiver efficiency on exergy efficiency**

**Figure 10. effect of receiver efficiency on system cost rate**

### 10. Effect of condenser output temperature

The effect of the condenser output temperature on the objective functions (energy efficiency, exergy efficiency, and cost rate) is shown in Figs. 11, 12 and 13, respectively. As shown in Fig. 11, an increase in the condenser output temperature reduces energy efficiency due to the decrease in system output energy for constant input energy. The same argument holds for the exergy efficiency of the system (Fig. 12). On the other hand, decreasing the system output energy decreases the capacity of the system components, which in turn results in lower system cost rates (Fig. 13).
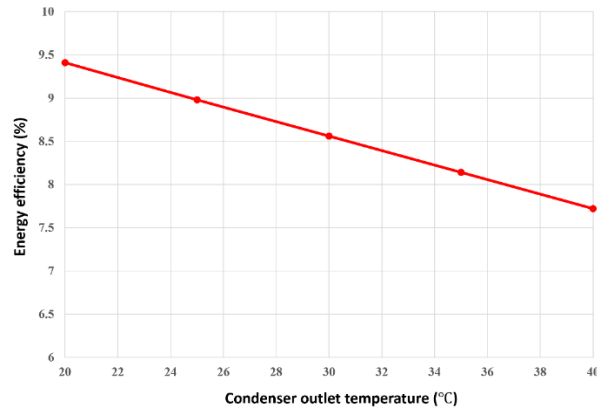


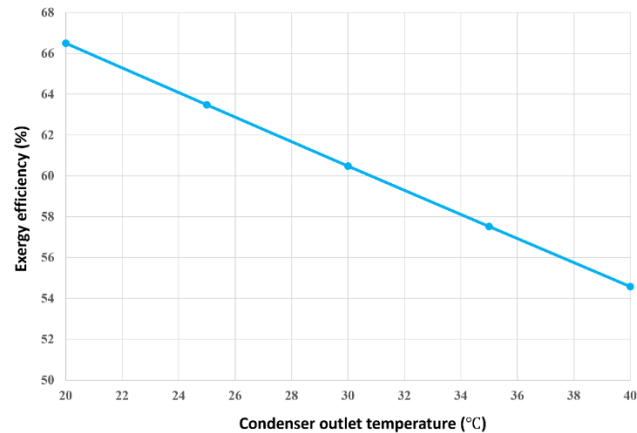**Figure 11. effect of condenser output temperature on energy efficiency**



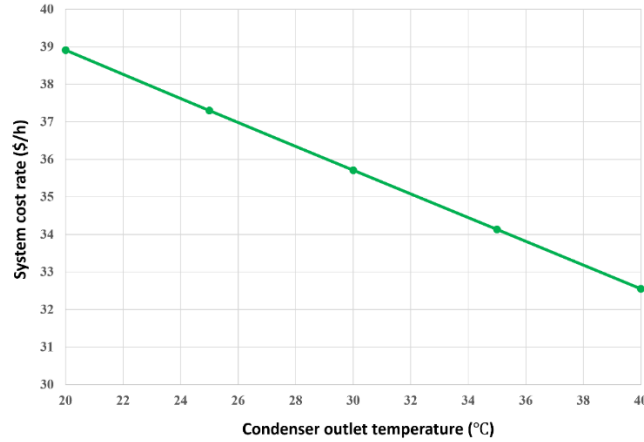**Figure 12. effect of condenser output temperature on exergy efficiency**

**Figure 13. effect of condenser output temperature on system cost rate**

### 11. Optimization results for the first scenario

Table 5 shows the results of multi-objective optimization for the first scenario compared to the base case. As shown in the table, multi-objective optimization for the first scenario increases energy efficiency and exergy efficiency by 22.32% and 8.61% respectively and increases the cost rate by 5.74%.

**Table 5. Results of the multi-objective optimization for the first scenario**

| Parameter | State | Value | Unit |
|---|---|---|---|
| Turbine inlet temperature | Base | 130 | °C |
| | Optimum | 149.8 | |
| Receiver efficiency | Base | 75 | % |
| | Optimum | 84.5 | |
| Condenser outlet temperature | Base | 25 | °C |
| | Optimum | 20.02 | |
| Energy efficiency | Base | 9.63 | % |
| | Optimum | 11.78 | |
| Exergy efficiency | Base | 63.48 | % |
| | Optimum | 68.95 | |
| Cost rate | Base | 140.41 | $/hour |
| | Optimum | 148.48 | |

### 12. Optimization results for the second scenario

Table 6 shows the results of multi-objective optimization for the second scenario compared to the base case. As shown in the table, multi-objective optimization for the second scenario reduces energy efficiency and exergy efficiency by 25.54% and 7.29%, respectively, while reducing the cost rate by 6.65%. Fig. 14 and Fig. 15 show the variation in energy efficiency, exergy efficiency, and cost rates for the first scenario and the second scenario in comparison with the base case.

674

**Table 6. Results of the multi-objective optimization for the second scenario**

| Parameter | State | Value | Unit |
|---|---|---|---|
| Turbine inlet temperature | Base | 130 | ℃ |
| | Optimum | 120.02 | |
| Receiver efficiency | Base | 75 | % |
| | Optimum | 60.3 | |
| Condenser outlet temperature | Base | 25 | ℃ |
| | Optimum | 30.52 | |
| Energy efficiency | Base | 9.63 | % |
| | Optimum | 7.17 | |
| Exergy efficiency | Base | 63.48 | % |
| | Optimum | 58.85 | |
| Cost rate | Base | 140.41 | $/hour |
| | Optimum | 131.07 | |
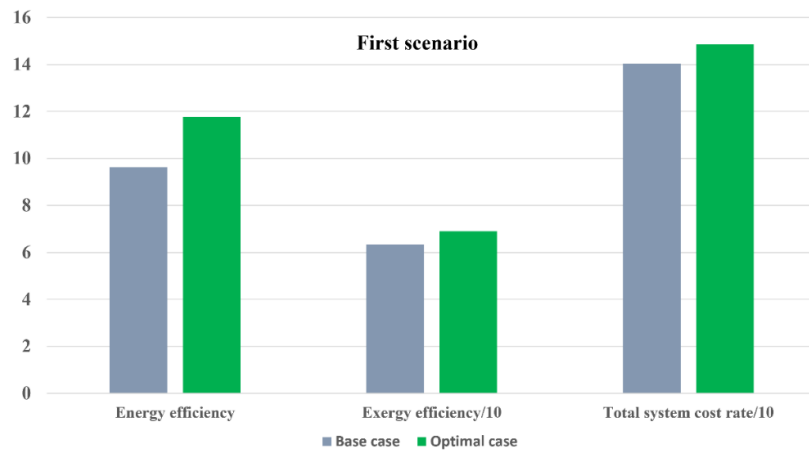


**Figure 14. Comparison of changes in system performance after optimization for the first scenario**
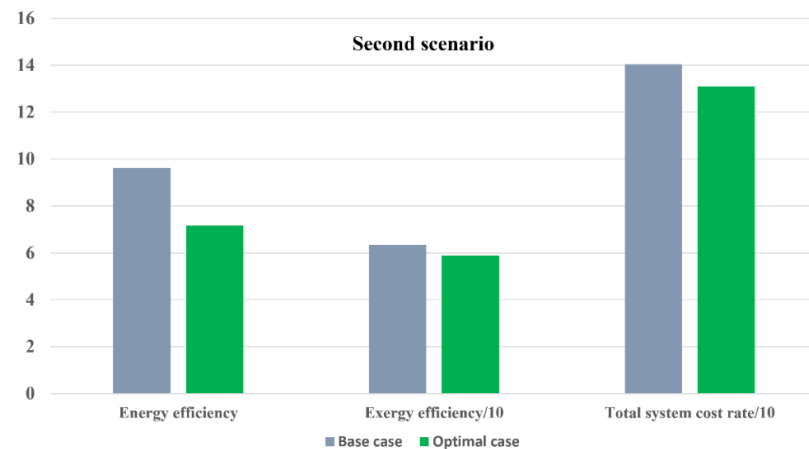


**Figure 15. Comparison of changes in system performance after optimization for the second scenario**

675

## 13. Conclusion

In this paper, a trigeneration system was simulated and optimized for a sustainable supply of heat, power, and cooling demands. Concentrated solar radiation was considered as the input energy of the system. The turbine inlet temperature, receiver efficiency, and condenser outlet temperature were selected as the decision variables in the optimization model. These variables were optimized using the PSO algorithm which resulted in maximum values of energy efficiency, exergy efficiency and system cost rate in two scenarios. In the first scenario, the purpose was to maximize the energy and exergy efficiency, and in the second scenario, the objective was to minimize the cost rate of the total system. The results of system optimization showed that energy efficiency and exergy efficiency increased by 22.32% and 8.61% in the first scenario, respectively. Moreover, the total cost rate of the system is reduced by 6.65% in the second scenario.

## References

[1] Y. Wang, Y. Shi, M. Ni, and N. Cai, "A micro tri-generation system based on direct flame fuel cells for residential applications," in *International Journal of Hydrogen Energy*, 2014, vol. 39, no. 11, pp. 5996–6005, doi: 10.1016/j.ijhydene.2014.01.183.

[2] G. Temir and D. Bilge, "Thermoeconomic analysis of a trigeneration system," *Appl. Therm. Eng.*, vol. 24, no. 17–18, pp. 2689–2699, Dec. 2004, doi: 10.1016/j.applthermaleng.2004.03.014.

[3] E. Cardona and A. Piacentino, "Optimal design of CHCP plants in the civil sector by thermoeconomics," *Appl. Energy*, vol. 84, no. 7–8, pp. 729–748, 2007, doi: 10.1016/j.apenergy.2007.01.005.

[4] J. Deng, R. Wang, J. Wu, G. Han, D. Wu, and S. Li, "Exergy cost analysis of a micro-trigeneration system based on the structural theory of thermoeconomics," *Energy*, vol. 33, no. 9, pp. 1417–1426, 2008, doi: 10.1016/j.energy.2008.05.001.

[5] H. Ghaebi, M. H. Saidi, and P. Ahmadi, "Exergoeconomic optimization of a trigeneration system for heating, cooling and power production purpose based on TRR method and using evolutionary algorithm," *Appl. Therm. Eng.*, vol. 36, no. 1, pp. 113–125, Apr. 2012, doi: 10.1016/j.applthermaleng.2011.11.069.

[6] V. Rezaee and A. Houshmand, "Energy and exergy analysis of a combined power generation system using PEM fuel cell and kalina cycle system 11," *Period. Polytech. Chem. Eng.*, vol. 60, no. 2, pp. 98–105, 2016, doi: 10.3311/ppch.8294.

[7] A. N. A. Mubin, M. H. Bahrom, M. Azri, Z. Ibrahim, N. A. Rahim, and S. R. S. Raihan, "Analysis performance of proton exchange membrane fuel cell (PEMFC)," in *IOP Conference Series: Materials Science and Engineering*, 2017, vol. 210, no. 1, doi: 10.1088/1757-899X/210/1/012052.

[8] K. K. T. Thanapalan, J. G. Williams, G. P. Liu, and D. Rees, "MODELLING OF A PEM FUEL CELL SYSTEM," *IFAC Proc. Vol.*, vol. 41, no. 2, pp. 4636–4641, 2008, doi: 10.3182/20080706-5-kr-1001.00780.

[9] I. Khazaee, M. Ghazikhani, and M. Mohammadiun, "Experimental and thermodynamic investigation of a triangular channel geometry PEM fuel cell at different operating conditions," *Sci. Iran.*, vol. 19, no. 3, pp. 585–593, Jun. 2012, doi: 10.1016/j.scient.2011.11.039.

[10] P. C. Chen, "The dynamics analysis and controller design for the PEM fuel cell under gas flowrate constraints," *Int. J. Hydrogen Energy*, vol. 36, no. 4, pp. 3110–3122, Feb. 2011, doi: 10.1016/j.ijhydene.2010.11.106.

[11] E. W. Saeed and E. G. Warkozek, "Modeling and Analysis of Renewable PEM Fuel Cell System," in *Energy Procedia*, 2015, vol. 74, pp. 87–101, doi: 10.1016/j.egypro.2015.07.527.

[12] S. Shiva Kumar and V. Himabindu, "Hydrogen production by PEM water electrolysis – A review," *Mater. Sci. Energy Technol.*, vol. 2, no. 3, pp. 442–454, Dec. 2019, doi: 10.1016/j.mset.2019.03.002.

[13] P. Ahmadi, I. Dincer, and M. A. Rosen, "Performance assessment and optimization of a novel integrated multigeneration system for residential buildings," *Energy Build.*, vol. 67, pp. 568–578, 2013, doi: 10.1016/j.enbuild.2013.08.046.

[14] M. Ni, M. K. H. Leung, and D. Y. C. Leung, "Energy and exergy analysis of hydrogen production by a proton exchange membrane (PEM) electrolyzer plant," *Energy Convers. Manag.*, vol. 49, no. 10, pp. 2748–2756, Oct. 2008, doi: 10.1016/j.enconman.2008.03.018.

[15] P. Ahmadi, I. Dincer, and M. A. Rosen, "Energy and exergy analyses of hydrogen production via solar-boosted ocean thermal energy conversion and PEM electrolysis," *Int. J. Hydrogen Energy*, vol. 38, no. 4, pp. 1795–1805, Feb. 2013, doi:

10.1016/j.ijhydene.2012.11.025.

[16]    M. Ebrahimi, A. Keshavarz, and A. Jamali, "Energy and exergy analyses of a micro-steam CCHP cycle for a residential building," *Energy Build.*, vol. 45, pp. 202–210, Feb. 2012, doi: 10.1016/j.enbuild.2011.11.009.

[17]    T. A. H. Ratlamwala, I. Dincer, and M. A. Gadalla, "Thermodynamic analysis of an integrated geothermal based quadruple effect absorption system for multigenerational purposes," *Thermochim. Acta*, vol. 535, pp. 27–35, May 2012, doi: 10.1016/j.tca.2012.02.008.

[18]    R. Moltames, B. Azizimehr, and E. Assareh, "Energy and Exergy Efficiency Improvement of a Solar Driven Trigeneration System Using Particle Swarm Optimization Algorithm," *J. Sol. Energy Res.*, vol. 4, no. 1, pp. 31–39, Jan.

2019, doi: 10.22059/JSER.2019.70905.

[19]    S. Elahifar, E. Assareh, and R. Moltames, "Exergy analysis and thermodynamic optimisation of a steam power plant-based Rankine cycle system using intelligent optimisation algorithms," *Aust. J. Mech. Eng.*, 2019, doi: 10.1080/14484846.2019.1661807.

[20]    B. Azizimehr, E. Assareh, and R. Moltames, "Thermoeconomic analysis and optimization of a solar micro CCHP by using TLBO algorithm for domestic application," *Energy Sources, Part A Recover. Util. Environ. Eff.*, 2019, doi: 10.1080/15567036.2019.1604883.

[21]    C. Yilmaz, "Thermoeconomic modeling and optimization of a hydrogen production system using geothermal energy," *Geothermics*, vol. 65, pp. 32–43, Jan. 2017, doi: 10.1016/j.geothermics.2016.08.008.